Energy Proceedings
Vol 49, 2024
ISSN 2004-2965

Visualization Experimental Investigation on Sanding Characteristics and Oil Production Capacity of Unconsolidated Sandstone Reservoirs#

Xuechen Tang[1,2*], Zihao Li[1,2], Jinxin Cao[1,2], Xinji Du[1,2], Yaqian Zhang[1,2], Tao Song[1,2], Qihang Li[1,2], Yiqiang Li[1,2]

1 State Key Laboratory of Petroleum Resources and Engineering, China University of Petroleum (Beijing), Beijing 102249, PR China

2 College of Petroleum Engineering, China University of Petroleum (Beijing), Beijing 102249, PR China
(Corresponding Author: tangxuechen1994@163.com)

ABSTRACT

Macroscopic sand production laws often fail to reveal the microscopic essence of sand production. To investigate the microscopic sand production process and oil production capacity of unconsolidated sandstone reservoirs, a visual plate model was designed to explore the influence of displacement rate and oil viscosity. Results show that the evolution of the sanding channel undergoes three stages: "migration initiation-channel formation-channel expansion". The corresponding fractal dimension increases initially, then decreases, and finally stabilizes. The sand production strength increases with the displacement rate and oil viscosity, but there is a critical value beyond which the strength increases sharply. These preliminary microscopic sand production morphologies and mechanisms provide important guidance for simulating microscopic sand production processes and quantitatively predicting sand production laws.

Keywords: visual sanding experiment, unconsolidated sandstone reservoirs, displacement rate, oil viscosity, oil production.

NONMENCLATURE

Abbreviations	
O&G	Oil and Gas
Symbols	
D_f	Fractal Dimension

1. INTRODUCTION

Hydrocarbons are the primary energy source due to exponential population growth and rapid industrialization.[1,2] Unless alternative energy sources are developed, hydrocarbons will continue to dominate the energy market.[3] According to statistics, about 70% of the world's oil and gas (O&G) reserves come from weakly consolidated or unconsolidated sandstone reservoirs.[4,5] Therefore, understanding the sand production process is essential.[6] Most physical simulation experiments focus on the macroscopic relationship between particle washout by fluid injection and the pressure differential across the core, predicting critical conditions and overall sand production laws.[7] However, these experiments fail to reveal the microscopic nature of particle migration and channel evolution.

Recent micro/meso-scale visualization experiments have become crucial in sand production mechanism research.[8,9] These experiments can observe fluid flow and particle migration in porous media, revealing the microscopic sand production processes and mechanisms in weakly cemented reservoirs. This paper designs a visual plate model combined with image processing technology to clarify the influence of displacement rate and oil viscosity on sanding characteristics and oil production capacity in unconsolidated sandstone reservoirs.

2. MATERIAL AND METHODS

2.1 Materials and model preparation

Materials used include 2.5 mm glass beads, sand grains (100-200 mesh), model oil with different viscosities, distilled water, methylene blue (from Shanghai Aladdin Biochemical Technology Co. Ltd.), and Sudan III (from Shanghai Macklin Biochemical Technology Co. Ltd.). The visualized model, shown in Fig. 1, consists of an inner cavity measuring 16 cm per side and 2.5 mm in height, created using acrylic plates sealed with a silicone gasket. An injector and a producer were set on the upper acrylic plate. The inner cavity was divided into a sand migration observation area and a sand production observation area. Glass beads were adhered to the bottom acrylic plate with double-sided tape, and sand particles were spread evenly. The model

This is a paper for the 16th International Conference on Applied Energy (ICAE2024), Sep. 1-5, 2024, Niigata, Japan.

was then reinforced with bolts to complete the visual model.

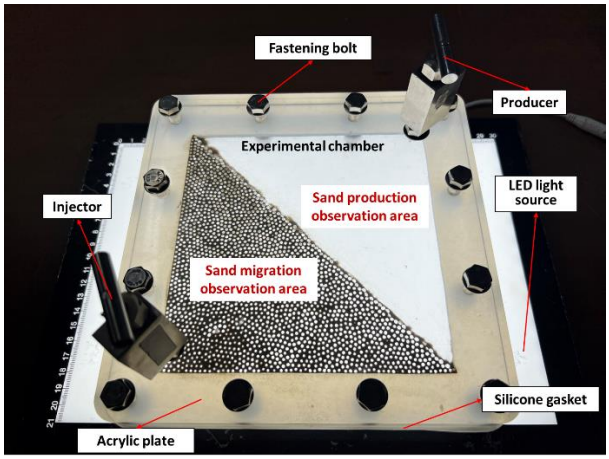

Fig. 1 Visualized model of sand migration experiment

2.2 Effect of displacement rate on sanding characteristics and oil production ability

In this section, six experiments were conducted with varying displacement rates (1, 3, 5, 8, 10, and 15 mL·min^{-1}). The specific experimental procedure was as follows: (1) fill the model and record the amount of sand used; (2) vacuum the model and saturate it with Sudan III-stained model oil (50 mPa·s); (3) conduct the test at the set displacement rate until no oil is produced; (4) record the entire experimental process with a high-speed camera; (5) perform image processing (Fig. 2) and record the volume of oil and water in the produced liquid and the dry weight of the sand in the sand production observation area to analyze the sanding characteristics and oil production capabilities.

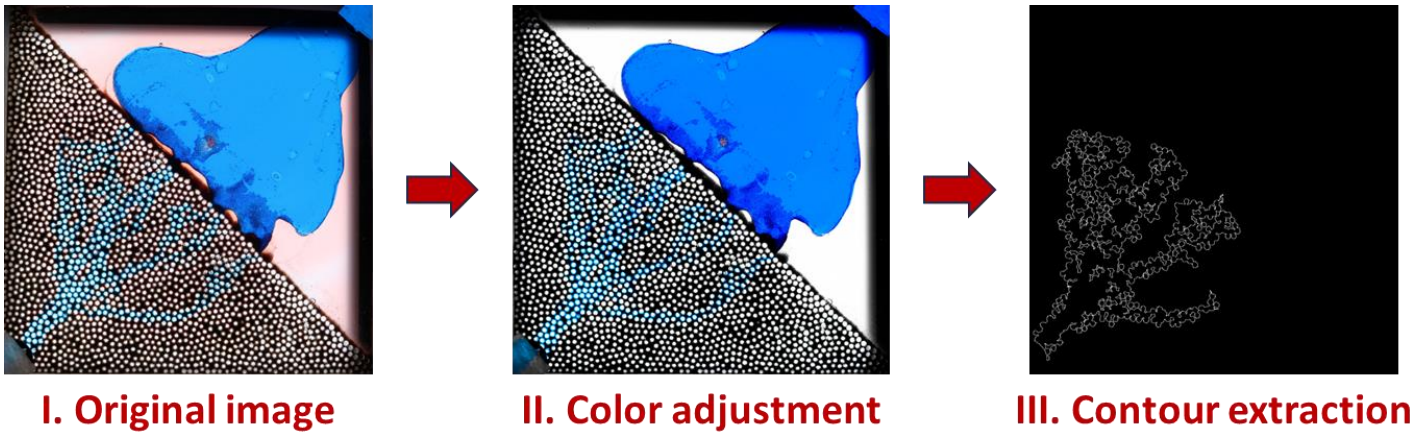

Fig. 2 Image processing

2.3 Effect of oil viscosity on sanding characteristics and oil production ability

Five experiments were conducted following the same procedure as described in Section 2.2. The difference was the use of model oil with varying viscosities (1, 25, 50, 100, 200 mPa·s), while keeping the displacement rate constant at 10 mL·min^{-1}.

3. RESULTS AND DISCUSSION

3.1 Effect of displacement rate on sanding characteristics and oil production ability

3.1.1 Formation process of sanding channel under different displacement rates

Fig. 3 illustrates the formation process of sanding channels under different displacement rates. The change in the fractal dimension (D_f) follows a pattern: it increases initially, then decreases, and finally stabilizes over time. Before the sanding channel is formally established, the channel contour expands continuously, causing the D_f to rise sharply. When the first channel reaches the boundary, the D_f reaches its maximum. After the local breakthrough, some branch channels disappear, leading to a decrease in D_f. Subsequently, the primary channel continues to expand until it stabilizes, the contour irregularity diminishes, and the D_f gradually decreases until it reaches a final stable value. Combining this pattern with the velocity field distribution obtained by PIV Lab, the evolution of the sanding channel undergoes three stages: “migration initiation-channel formation-channel expansion”, as shown in Fig. 4. Additionally, the time at which the maximum D_f value appears advances with increasing displacement rates, indicating that higher displacement rates accelerate the breakthrough of sanding channels. Moreover, there is a critical displacement rate of 5 mL·min^{-1}, at which the channel achieves the highest D_f value of 1.438, indicating the most complex channel contour.

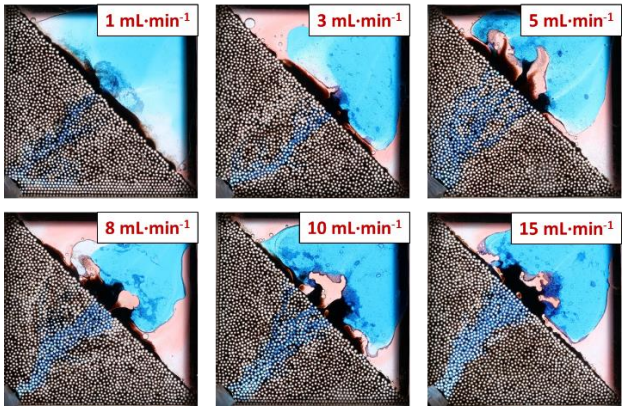

(a) Distribution of oil, water, and sand at the end of displacement

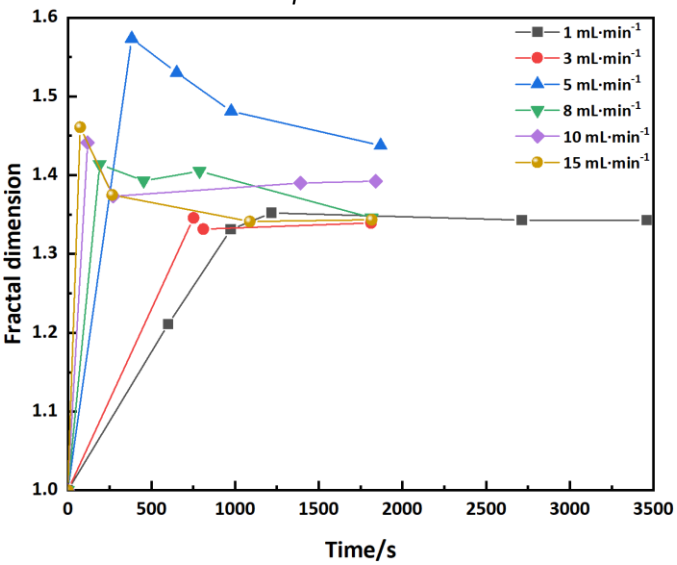

(b) Fractal dimension change of channel contour with time

Fig. 3 Formation process of sanding channel under different displacement rates

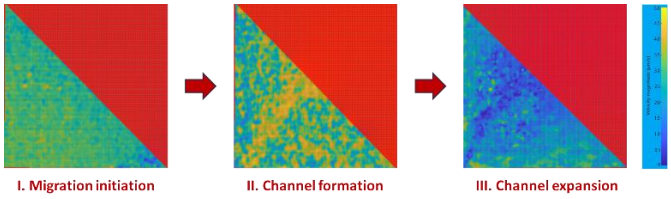

Fig. 4 Three stages of the formation of sanding channel obtained by PIV Lab

3.1.2 Proportion of sand-producing influence area under different displacement rates

To quantitatively describe the proportion of sand-producing areas, MATLAB was used to further process Fig. 3a. As described in the left figure of Fig.5, the area affected by methylene blue-stained water is filled with white, representing the actual sand-producing region, while the rest is filled with black. The black portion enclosed within the white area represents the remaining oil in the sand-producing region. Together, these two parts are referred to the sand-producing influence region, as illustrated in the right figure of Fig. 5. By using MATLAB to determine the actual number of pixels in each region and calculating the ratio of these pixel counts to the total number of pixels in the sand migration observation area, the proportions of each region can be obtained.

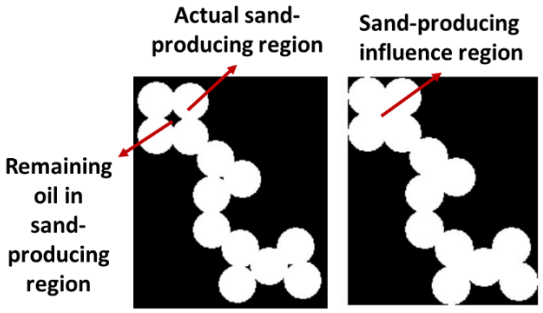

Fig. 5 sand-producing influence region described by the binary image

As shown in Fig. 6, the change in the proportion of the sand-producing influence region with respect to the displacement rate follows the same trend as the D_f. The influence region reaches its maximum proportion at 5 mL·min^{-1}, accounting for 36.13%. The broken line indicates that the actual sand-producing region constitutes the majority of the influence region, ranging from 77% to 98%. Combining Fig. 6 with Fig. 3a, it is evident that, except for the significant distribution of remaining oil at 5 mL·min^{-1}, the remaining oil in the influence region at other displacement rates is mostly scattered.

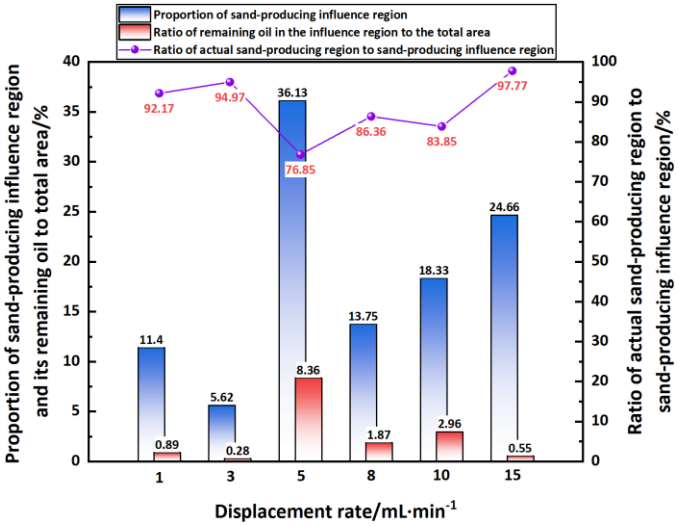

Fig. 6 Proportion of sand-producing influence region and remaining oil content under different displacement rates

3.1.3 Final displacement results under different displacement rates

The relationship between oil recovery, sand production rate, and displacement rate is illustrated in Fig. 7. The initial saturated oil volume of the model is approximately 40 mL. As the displacement rate increases, the produced oil volume gradually decreases from 32.7 mL at 1 mL·min^{-1} to 20.7 mL at 15 mL·min^{-1}, resulting in a decrease in oil recovery from 81.34% to 51.75%, a drop of 29.59 percentage points. The initial saturated sand volume is approximately 17.5 g. With the increase in injection rate, the sand production of the model gradually increases from 1.41 g at 1 mL·min^{-1} to 3.34 g at 15 mL·min^{-1}, leading to an increase in the sand production rate from 8.13% to 18.75%.

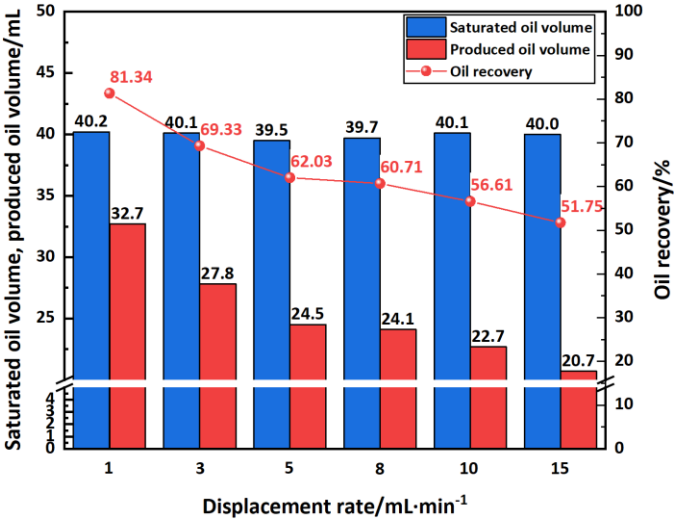

(a) oil recovery

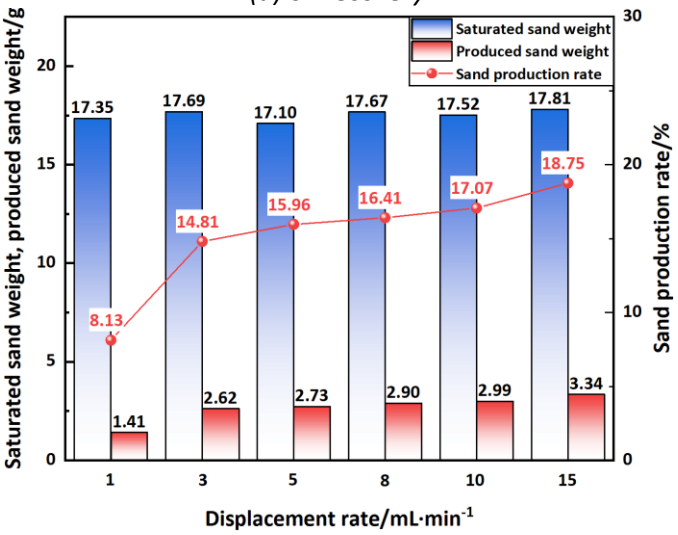

(b) sand production rate

Fig. 7 Relationship between oil recovery and sand production rate with displacement rate

However, the overall effect of sand production on the displacement process cannot be accurately described solely by the oil recovery and the sand production rate. Therefore, the sanding intensity index S is defined to comprehensively reflect the sand-oil ratio (V_s/V_o) and the sand sweep degree (A_s/A_w):

$$S = \frac{V_s}{V_o} \cdot \frac{A_s}{A_w} \times 100 \quad (1)$$

where V_s is the sand production volume, mL; V_o is the produced oil volume, mL; A_s is the area proportion of sand-producing influence area; A_w is the proportion of water flooding swept area.

As shown in Fig. 8, the sand-oil ratio gradually increases with the displacement rate, indicating that higher displacement rates cause the sand content in the output to become more dominant. With the increase in displacement rate, the sand sweep degree fluctuates, reaching a peak at 5 mL·min^{-1}. Consequently, the sanding intensity index, which encapsulates both the sand-oil ratio and the sand sweep degree, also exhibits a fluctuating rise, and there is a critical displacement rate, leading to a sharp increase.

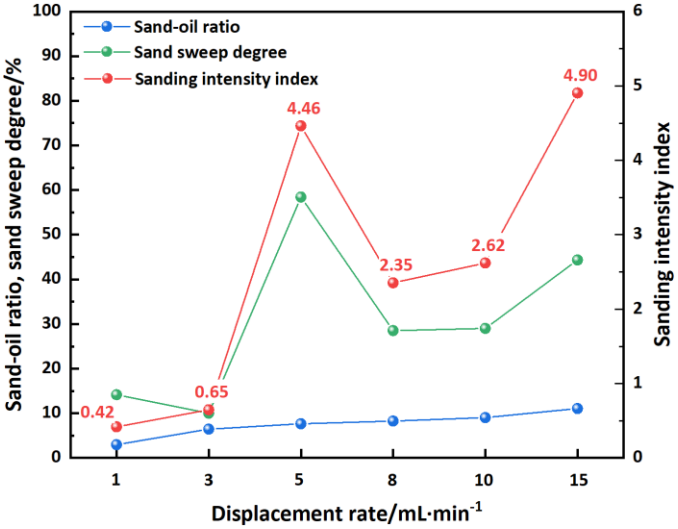

Fig. 8 Sanding intensity index as a function of displacement rate

3.2 Effect of oil viscosity on sanding characteristics and oil production ability

3.2.1 Formation process of sanding channel under different oil viscosity

Fig. 9 shows the formation process of sanding channel under different oil viscosity. The D_f of each time increases with the increase of oil viscosity, indicating that the complexity of the sanding channel increases significantly; moreover, the maximum value of D_f appears earlier with the increase of oil viscosity due to viscous fingering; Furthermore, it can be found that the development of D_f under low viscosity conditions is mainly due to the stripping of surrounding sand particles

by sand channels, while under high viscosity conditions, it is due to the increase of channel number.

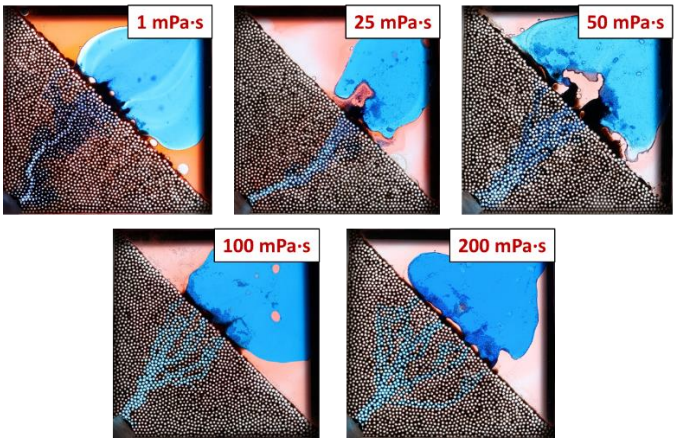

(a) Distribution of oil, water, and sand at the end of displacement

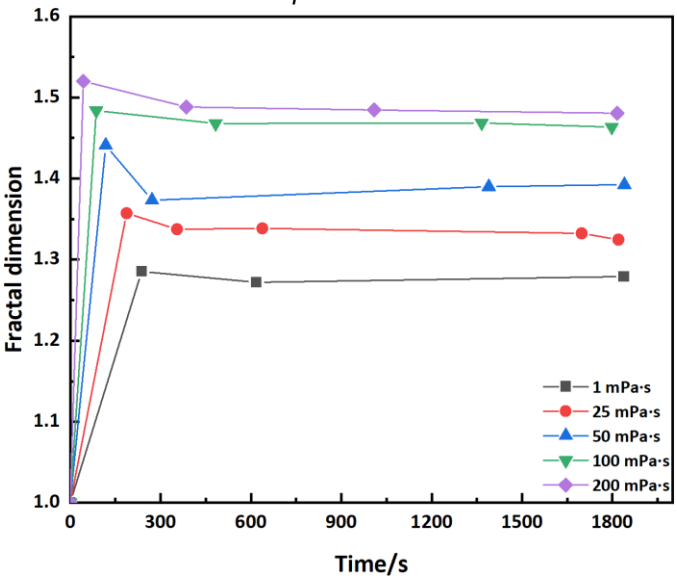

(b) Fractal dimension change of channel contour with time

Fig. 9 Formation process of sanding channel under different oil viscosity

3.2.2 Proportion of sand-producing influence area under different oil viscosity

As illustrated in Fig. 10, consistent with the change rule of D_f, the proportion of sand-producing influence region increases with increasing oil viscosity. The ratio of the actual sand-producing region to the sand-producing influence region decreases first and then increases with the increase of oil viscosity and finally tends to be stable. Combined with Figs. 9a and 10, when the oil viscosity is low, the remaining oil in the influence region is mainly distributed in the thick and large channels in the form of dots, and the overall content is small; when the viscosity is high, the remaining oil in the influence region is mainly distributed in the form of blocks between the branch channels, and the content is relatively large.

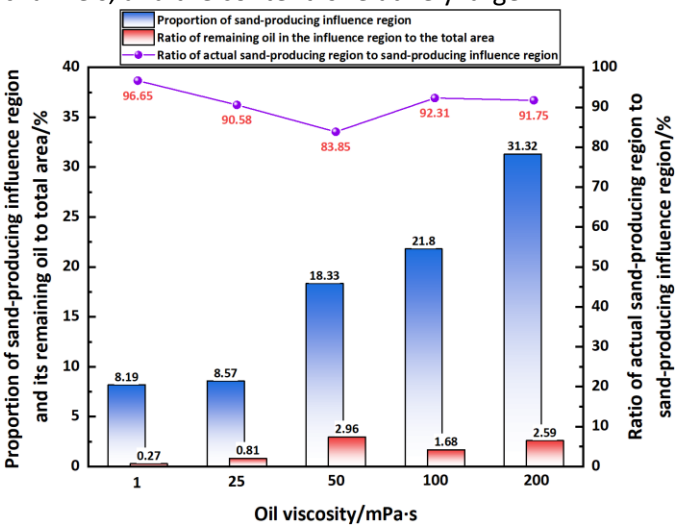

Fig. 10 Proportion of sand-producing influence region and remaining oil content under different oil viscosity

3.2.3 Final displacement results under different oil viscosity

As shown in Fig. 11, the relationship between oil recovery, sand production rate, and oil viscosity is detailed. As oil viscosity increases, the produced oil volume gradually decreases from 26.0 mL at 1 mPa·s to 15.0 mL at 200 mPa·s, and the oil recovery drops from 65.49% to 37.88%, a decrease of 27.61 percentage points. However, there is a critical viscosity at which the sand production rate significantly increases to 17.07%. Overall, the sanding intensity index exhibits an upward trend with increasing oil viscosity, but there is a critical viscosity at which the intensity index sharply increases, as shown in Fig. 12.

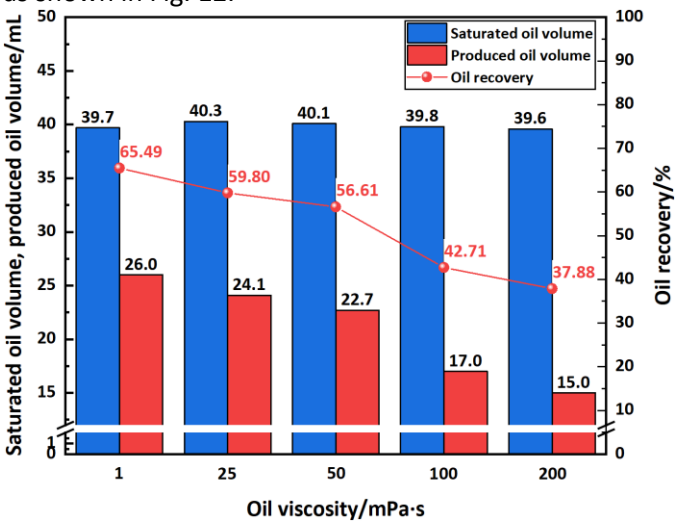

(a) oil recovery

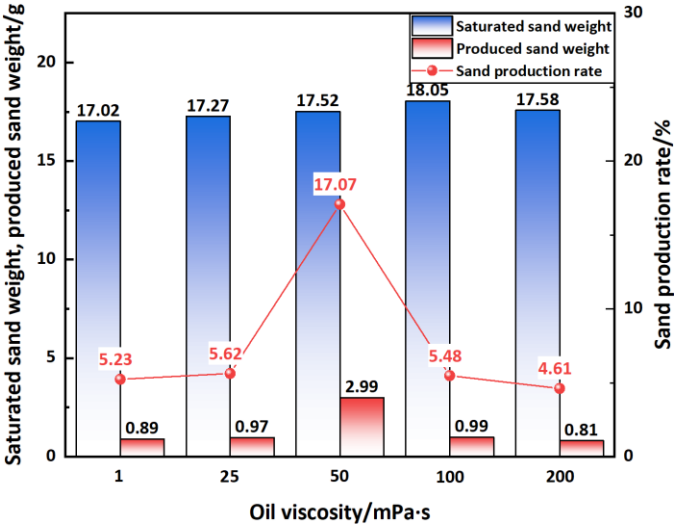

(b) sand production rate

Fig. 11 Relationship between oil recovery and sand production rate with oil viscosity

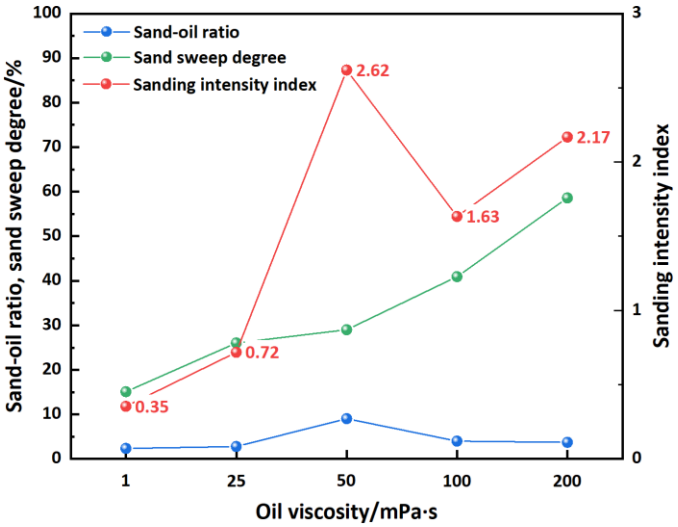

Fig. 12 Sanding intensity index as a function of oil viscosity

4. CONCLUSIONS

Sand production in unconsolidated sandstone reservoirs is a complex phenomenon, which depends on various factors. We present a visualized model in this work to discuss the influence of displacement rate and oil viscosity. Specific conclusions are as follows:

1. A visual experimental equipment for studying sand production characteristics and oil production capacity was designed and manufactured;

2. The evolution of the sanding channel undergoes three stages: “migration initiation-channel formation-channel expansion”. The fractal dimension initially increases, then decreases, and finally stabilizes.

3. The sand production intensity increases with the displacement rate and oil viscosity. However, there is a critical value at which the sand production intensity increases sharply.

ACKNOWLEDGEMENT

The authors thank the National Natural Science Foundation of China (Grant U23B6003) for the support of this work.

REFERENCES

[1]A. Al Adasani and B. Bai, Analysis of EOR projects and updated screening criteria," J. Pet. Sci. Eng. **79**(1), 10-24 (2011).

[2]X. Tang, Y. Li, J. Cao, Z. Liu, X. Chen, L. Liu, Y. Zhang, and Q. Li, "Adaptability and enhanced oil recovery performance of surfactant–polymer flooding in inverted seven-spot well pattern," Phys. Fluids. **35**(5) (2023).

[3]N. Pal and A. Mandal, "Oil recovery mechanisms of Pickering nanoemulsions stabilized by surfactant-polymer-nanoparticle assemblies: A versatile surface energies’ approach," Fuel. **276**, 118138 (2020).

[4]B. Zhou, C. Dong, Y. Song, X. Zhan, G. Gwamba, and H. Bai, "Visualization-based experimental investigation of microscopic sand production characteristics and mechanisms in weakly consolidated sandstone reservoirs," Geoenergy Sci. Eng. **229**, 212054 (2023).

[5]D. Garolera, I. Carol, and P. Papanastasiou, "Micromechanical analysis of sand production," Int. J. Numer. Anal. Methods Geomech. **43**(6), 1207-1229 (2019).

[6]M. He, X. Luo, F. Yu, P. Xia, Z. Teng, and C. Wang, "Influence of Sand Production Damage in Unconsolidated Sandstone Reservoirs on Pore Structure Characteristics and Oil Recovery at the Microscopic Scale," Acs Omega. **7**(44), 40387-40398 (2022).

[7]X. Nie, S. Yang, J. Ding, L. Cao, F. Zhou, Q. Ma, and Z. Qiu, "Experimental investigation on permeability evolution law during sand production process of weak sandstone," J. Nat. Gas Sci. Eng. **21**, 248-254 (2014).

[8]Y. Song, C. Dong, B. Zhou, X. Zhan, and G. Gwamba, "Experimental simulation of wormhole sanding cavity pattern and microscopic mechanism in heterogeneous weakly-cemented sandstone," J. Pet. Explor. Prod. Technol. **13**(6), 1519-1534 (2023).

[9]C. Dong, B. Zhou, F. Huang, L. Zhang, Y. Zhao, Y. Song, and J. Deng, "Microscopic sand production simulation and visual sanding pattern description in weakly consolidated sandstone reservoirs," Pet. Sci. **19**(1), 279-295 (2022).